Defensive Architecture of the Mediterranean / Vol. XIII / Bevilacqua, Ulivieri (Eds.)

DOI: 10.12871/978883339794848

Integrated use of ground penetrating radar and time domain reflection for volumetric water content evaluation in wood structures inside the castle of Carosino (Taranto, Italy)

Dora Francesca Barbolla[a], Lara De Giorgi[b], Lucrezia Longhitano[c], Chiara Torre[d], Giovanni Leucci[e]

[a] Institute of Heritage Science (ISPC) National Research Council (CNR), Lecce, Italy, dora.barbolla@ispc.cnr.it; [b] Institute of Heritage Science (ISPC) National Research Council (CNR), Lecce, Italy, lara.degiorgi@cnr.it; [c] University of Catania, Catania, Italy, lucrezia.longhitano@phd.unict.it; [d] University of Catania, Catania, Italy, chiara.torre@phd.unict.it, [e] Institute of Heritage Science (ISPC) National Research Council (CNR), Lecce, Italy, giovanni.leucci@cnr.it

Abstract

Ground-penetrating radar (GPR) and time domain reflectometry (TDR) was used to estimate the dielectric permittivity and successively the volumetric water content of several types of wood. An empirical relationship was found between the dielectric constant and volumetric water content. Results were applied to a case study of the Castle of Carosino (Taranto, Italy).

Keywords: TDR, GPR, Carosino Castle.

1. Introduction

The electromagnetic characteristics of the wood are of great interest within GPR prospecting related to the study of the conservation state of the wooden structures. In particular, these characteristics, if correctly retrieved, allow not only a correct time-depth conversion (Daniels, 2004) but also a correct focusing of the buried targets (such as voids, knots, etc.) through migration or, more in general, an inversion algorithm (Leucci et al. 2007).

Moreover, depending on the applications, the characteristics of the medium can be crucial in themselves and not only in relationship to the reconstruction and interpretation of the targets. This can happen, e.g. when the "final" quantity of interest is the water content of the wood (Topp et al. 1980). In general, the dielectric permittivity and the electrical conductivity of the embedding medium depend in a meaningful way, but also in a complicated and often unknown way, on the chemical, physical and mineralogical properties mixture composing the wood at hand. This makes it quite hard to get a reliable a-priori knowledge of them. In particular, some experimental values or semi-empirical laws are available (Daniels, 2004; Jol, 2009); nevertheless, they should be considered reference-average quantities, which are helpful to test the likelihood of a measure in the field but should not replace it.

In particular, the measure of the dielectric permittivity of the wood can be performed from the same GPR data (Lambot et al. 2004; Soldovieri et al. 2008), classically using the shape of the diffraction curves. Alternatively, the dielectric permittivity can be evaluated through the time domain reflectometry (TDR) technique (Cataldo et al. 2011).

In this paper, a comparative experimental evaluation of the dielectric permittivity of some wood samples is proposed. Results show an excellent agreement between the diffraction curve method analysis and the TDR measurements.

An empirical relationship was found between dielectric constant and volumetric water content in the wood structures. Results were applied to a case study to study the conservation state of the wood beams of the castle of Carosino (Apulia region, south Italy).

2. TDR Measurements

The experimental setup for TDR measurements included a TDR unit (Campbell Scientific TDR100), a non-invasive three-rod probe and a 3.5 m-long 50 Ω-matched coaxial cable that connected the probe to the TDR unit. The TDR100 generates a step-pulse signal with a rise-time of 200 ps, which corresponds to a frequency bandwidth of approximately 1.7 GHz. The wood samples have been dehydrated at 105 Celsius for 24 hours. In particular, drying wood prevents inhomogeneity due to possible gradients of moisture content. Moreover, dehydration also reduces the dependence of the permittivity on potential gradients of density. Successively the samples were immersed in water and saturated. The relative dielectric permittivity of the prepared sample was determined through the well-known TDR method (Robinson et al. 2003). In TDR measurement, the step-pulse signal generated by the TDR unit propagates along the probe inserted in the material under test; the reflected signal is acquired by the same TDR unit and displayed in terms of reflection coefficient, a function of the apparent distance in the air.

As detailed in ref. (Cataldo et al. 2009), for low-loss and low-dispersive materials, the relative dielectric permittivity can be evaluated through the following equation:

$$\varepsilon \cong \left(\frac{L_{app}}{L_{phys}} \right)^2 \qquad (1)$$

where Lapp is the apparent distance of the probe inserted in the sample under test (Lapp is calculated directly from the TDR waveform), and Lphys is the probe's physical (actual) length.

According to ref. (Balestrieri et al. 2012), the accurate value of Lphys was evaluated through preliminary TDR measurements performed in air and distilled water (this was necessary because a tiny portion of the sensing element is contained in a Teflon cap, and this portion must be correctly subtracted to obtain the actual value of Lphys).

For the case considered herein, reference TDR measurements were performed using the non-invasive three-rod probe. For each acquisition, the instrumental averaging number was 128. The number of sample points for each waveform was 2,048.

For example, Fig. 1 shows one of the acquired TDR waveforms and the corresponding first derivative curve. The derivative facilitates the evaluation of Lapp; in fact, the first peak of the derivative (occurring approximately at 6.2 cm) corresponds to the beginning of the probe, whereas the second one (occurring around 5.5 cm) corresponds to the open-ended probe termination.

The relative dielectric permittivity of the sand, calculated through equation (1) and averaged over the four measurement points in the tank, is 4.01 (evaluated with a corresponding expanded uncertainty of 3%).

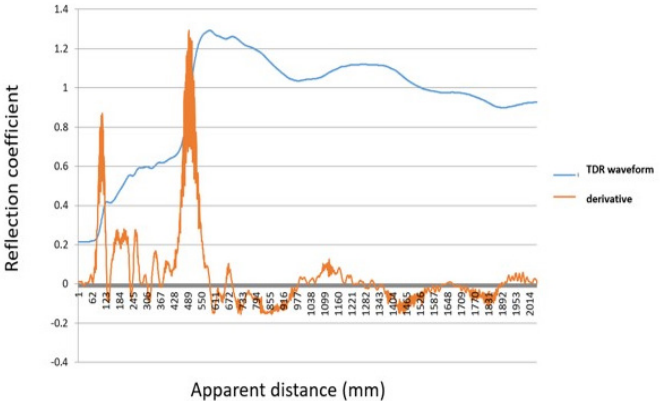

Fig. 1- The location of geophysical surveys TDR waveform (blue curve) and corresponding first derivative (orange curve) obtained for the wet maple (graphic elaboration by authors)

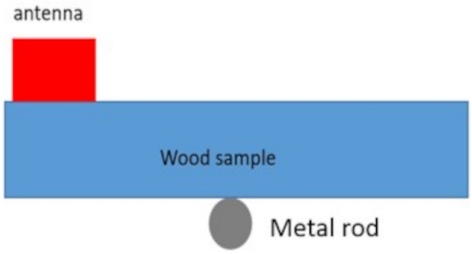

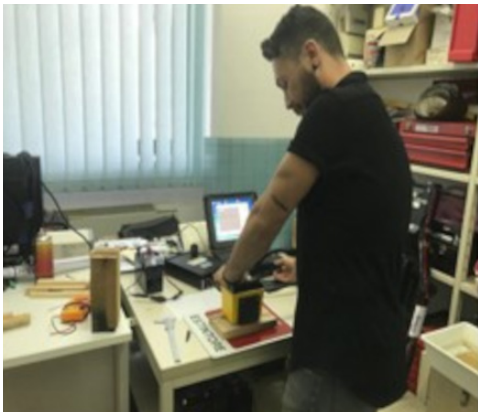

Fig. 2 - GPR experimental setup (photo by Giovanni Leucci)

3. GPR measurements

The measurements have been performed with an IDS Ris Hi-mode system equipped with an antenna at a nominal central frequency of 2 GHz. Each B-scan has a time window of 32 ns, discretized using 2048 samples. When moving the antenna on the wood, extreme care was taken to pull the antenna at a constant velocity. The repetition of the scan along the same line three times has allowed a test about the uniformity of the antenna movement velocity. For GPR measurements, the experimental setup was a wooden sample on a metal rod (Fig. 2). This allows us to analyse the data using the diffraction curve method.

The diffraction curve method is based on the matching between the data and a model describing the two-way time of the GPR signal. This model provides a curve while considering the movement of the antenna over the target. In particular, given an electrically tiny target (in our case, the bar with the small cross-section in terms of the probing wavelength) at the abscissa , if the offset between the transmitting and receiving antennas is neglected, concerning fig. 2, the model for the diffraction curve is given by (Leucci, 2019)

$$t = \frac{2}{c}\sqrt{(x - x_o)^2 + \left(\frac{t_o}{2}\right)^2} \qquad (2)$$

where c is the propagation velocity in the soil, linked to the relative permittivity ε_s by the well-known relationship

$$c = \frac{c_o}{\sqrt{\varepsilon_s}}$$

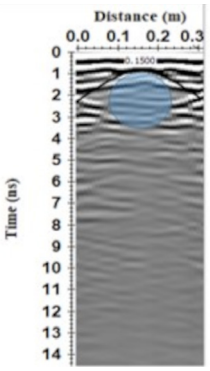

Fig. 3 - GPR radar section with the diffraction curve analysis (graphic elaboration by authors)

and t_o is the minimum recorded time, gathered when the source-observation point flies just over the target so that $x = x_o$.

The diffraction curve analysis (Fig. 3) allows esteeming the electromagnetic wave velocity and successively the dielectric constant.

The diffraction curve adaptation done a velocity of 0.15m/ns. Using the relationship

$$c = \frac{c_o}{\sqrt{\varepsilon_s}}$$

is possible to calculate the dielectric constant. In this case, a ε=4 is obtained. Analysing the results obtained on the different samples with TDR and GPR, the relationship between dielectric constant and volumetric content in water is obtained (Fig. 4).

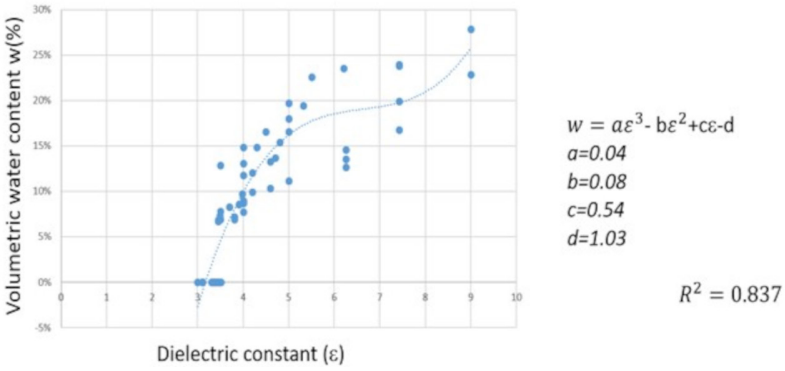

Fig. 4- GPR Relationship between dielectric constant and volumetric water content (graphic elaboration by authors)

4. The case study: the castle of Carosino

The Castle (Fig. 5) was built in the 15th century by the noble Simonetta family, the ducal palace is the heart of the ancient fief of Carosino in the centre of the ancient village. After the renovations carried out by the Spanish counts D'Ayala-Valva in the late 19th century, the castle took on the appearance of an ancient Renaissance manor bordered by refined battlements and developed around a square courtyard from which the stairways leading to the first floor where the large halls with barrel or cross vaults follow one another. Since 1895 the building has been owned by the Municipality and is used as a cultural container for the city.

To help the restoration work, GPR surveys were carried out on some wooden elements making up the ceiling beams. All GPR profiles were performed on wooden structures (Fig. 6) and acquired used the georadar Ris-Hi-mod with the 2GHz antenna at 1024 samples/track; the other acquisition parameters were optimized on-site and held constant for each profile. To eliminate the noise component present in the data, facilitating the interpretation, processing was realized whose phases are listed below: i) background removal; ii) migration. The presence of various anomalies due to small inhomogeneities, such as nodes and fractures, make possible a rapid and accurate analysis of the velocity of propagation of electromagnetic waves and allowed to obtain the depth of the anomalies.

The GPR data (Fig. 7) show that: the radar signal has an excellent penetration and crosses

Fig. 5- The Castle of Carosino (Image Landsat/Copernicus Data Sio, NOAA US Navy, NGA, GEBCO Image © 2022 TerraMetrics; and photo by Giovanni Leucci)

the element investigated for all its thickness; the surface portion of the wooden structures, for a thickness varying from 0.22 to 0.25 m, is generally characterized by reflections of weak amplitude, and this testifies to a net decrease in the density of the wood, probably related to both the activity of wood-eating insects and chemical attack; this anomaly appears to be more extensive on the extrados of the chains where the infiltration of rainwater, in the presence of significant accumulations of guano, may have generated a corrosive action resulting in breakdown of the cellular elements of the wood; the numerous reflections in the shape of hyperbole, placed at various depths indicate hardening of woody tissue that, in size and shape, can be related to nodes, single or in groups, their number, sometimes high, determines an average density including between 3 and 5 nodes per meter, but in some elements of the apse area will reach higher values; reflections with continuous development are generated by sub-horizontal fissures almost always oriented in the direction of the grain; their width is generally close to 1 cm.

Fig. 6- The surveyed wooden structures (photo by Giovanni Leucci)

Using a point-source reflection from a buried object to determine the average velocity and the use of the relationship shown in Fig. 4 gives an accurate (qualitative) estimate of the volumetric water content (Fig. 8).

The average volumetric water content of the wood varies from about 5% to 10% (Fig. 8). Water content was also measured through a direct mode using a wooden core, and results agree with those obtained using our relationship.

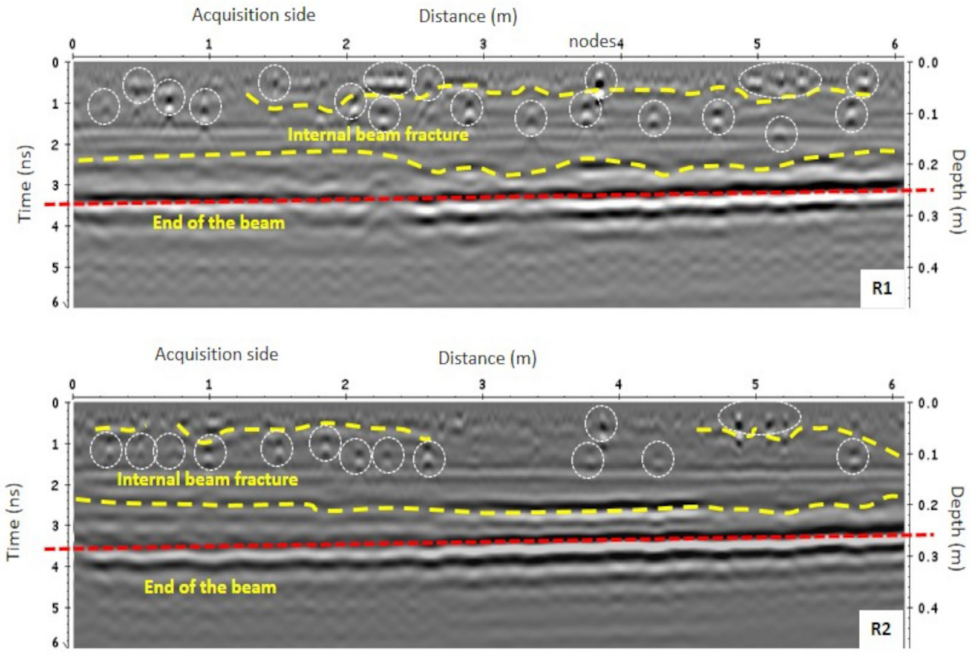

Fig. 7- The processed radar sectionssurveyed wooden structures (graphic elaboration by authors)

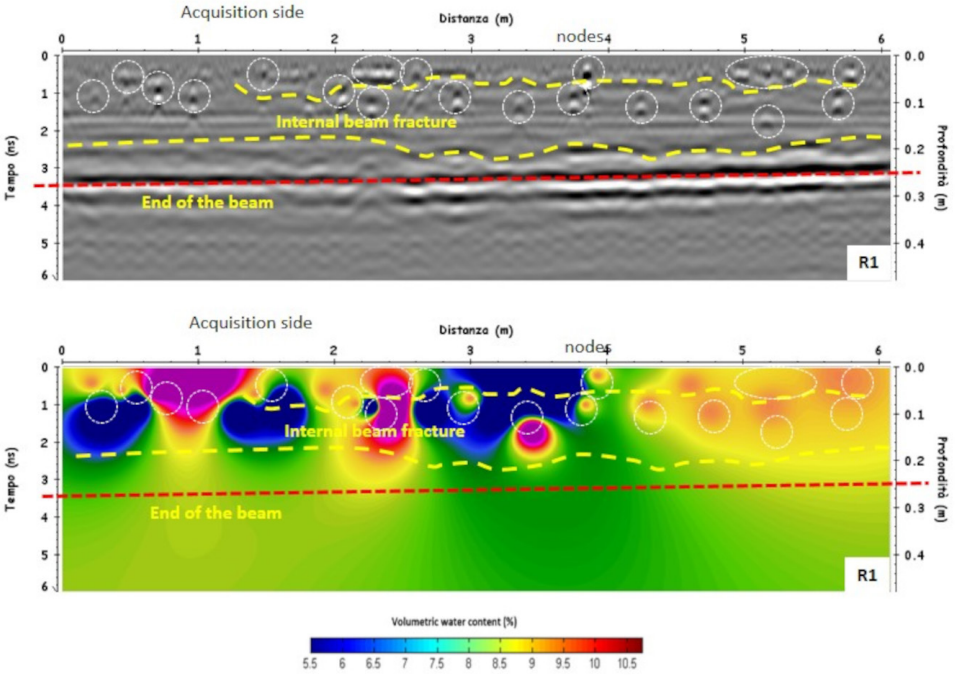

Fig. 8- The distribution of volumetric water content (graphic elaboration by authors)

5. Conclusions

In this paper, an experimental comparison between GPR and TDR measurements to determine the dielectric permittivity of a series of wood samples was proposed. A good correspondence, especially because (as it is easily calculable) was found between GPR and TDR measurements. A relationship between dielectric constant and volumetric water content was found. The GPR measurements on the case study allowed the presence of various abnormalities that correspond to nodes and/or slots, making possible a rapid and accurate analysis of the electromagnetic waves velocity of propagation and thus obtaining the depth of these anomalies. Among the main obtained data, it is worth stressing the following: the surface portion of the beams, for a thickness varying from 2 to 5-6 cm, is characterized by abnormalities related to the activity of wood-eating insects and chemical attacks due to pigeon droppings; the numerous reflections in the form of hyperbole, located at various depths, indicate that hardening of woody tissue can be mapped, both in size and shape, as nodes; the continuous reflections with a sub-horizontal development are generated by fissures almost always oriented in the direction of wood fibres.

Volumetric water content analysis shows an approximately homogeneous distribution of the moisture in the analysed woods elements.

References

Balestrieri, E., De Vito, L., Rapuano, S. & Slepicka, D. (2012) Estimating the uncertainty in the frequency domain characterization of digitizing waveform recorders. *IEEE Transactions on Instrumentation and Measurement*, 61(6), 1613-1624.

Cataldo, A., De Benedetto, E. & Cannazza, G. (2011) *Broadband reflectometry for enhanced diagnostics and monitoring applications*. Berlino, Springer Verlag.

Cataldo, A., Cannazza, G., De Benedetto, E., Tarricone, L. & Cipressa, M. (2009) Metrological assessment of TDR performance for moisture evaluation in granular materials. *Measurement*, 42(2), 254-263.

Daniels, D. J. (ed.) (2004) *Ground penetrating radar 2nd edition*. London, The Institution of Electrical Engineers.

Jol, H. (2009) *Ground Penetrating Radar: Theory and applications*. Amsterdam, Elsevier.
Lambot, S., Slob, E. C., van den Bosch, I., Stockbroeckx, B. & Vanclooster, M. (2004) Modeling of ground-penetrating radar for accurate characterization of subsurface electric properties. *IEEE Transactions on Geoscience and Remote Sensing*, 42(11), 2555-2568
Leucci, G., Persico, R. & Soldovieri, F. (2007) Detection of Fracture From GPR data: the case history of the Cathedral of Otranto. *Journal of Geophysics and Engineering*, 4, 452-461.
Leucci, G. (2019) *Nondestructive Testing for Archaeology and Cultural Heritage: A practical guide and new perspective.* Cham, Switzerland, Springer Nature Switzerland AG.
Robinson, D. A., Schaap, M., Jones, S. B., Friedman, S. P. & Gardner, C. M. K. (2003) Considerations for improving the accuracy of permittivity measurement using time domain reflectometry: air-water calibration, effects of cable length. *Soil Science Society of America Journal*, 67, 62-70.
Soldovieri, F., Prisco, G. & Persico, R. (2008) Application of Microwave Tomography in Hydrogeophysics: examples. *Vadose Zone Journal*, 160-170.
Topp, G. C., Davis, J. L. & Annan, A. P. (1980) Electromagnetic determination of soil water content: measurements in coaxial transmission lines. *Water Resources Research*, 16, 574-582.